CHAPTER VII

ENHANCEMENT OF SPECTRAL INTENSITIES OF MERCURY TRIPLET LINES IN LONGITUDINAL MAGNETIC FIELDS.

7.1. Introduction

Enhancement of spectral intensities in a magnetic field has long been observed (Rokhlin, 1939 in inhomogeneous longitudinal magnetic field, Forrest and Franklin, 1966 and Hegde and Ghosh, 1979 in longitudinal magnetic field, Kulkarni, 1944 and Sen, Das and Gupta, 1972 in transverse magnetic field). In transverse magnetic field it has been observed that as the magnetic field increases, the spectral intensities of lines increases and attaining a maximum value ~~of~~ at a certain magnetic field, gradually decreases. Sen et al (1972) have shown that the enhancement phenomenon can be quantitatively interpreted by the increase of electron temperature and decrease of radial electron density caused by the presence of a transverse magnetic field. In case of longitudinal magnetic field Hegde and Ghosh (1979) applied a collisional radiative model to the positive column of helium plasma and interpreted the enhancement of radiation with field.

In this chapter, investigation has been reported for enhancement of sharp series triplet radiations of mercury in longitudinal magnetic field. The sharp series

triplet lines have a common upper level. For transitions originating from the same upper level, the relative intensities do not depend on its excitation cross section, but only on the line strength. The signal strength at the detector should be proportional to emission rate integrated both along the detector line of sight and over the spectral profile and might be modified by any self absorption. Variation of signal strength with longitudinal magnetic field has been obtained in terms of variation of these parameters.

7.2. Experimental arrangement

Measurements were carried on the radiation enhancement of spectral lines in the sharp series triplets of mercury atoms in a low pressure mercury arcs placed in a longitudinal magnetic field. A d.c. vertical mercury arc was placed between the pole-pieces of an electromagnet. The arc was constructed of pyrex tube of 0.75 cm. internal radius and 8 cm. in length and was forced cooled externally. The buffer gas was dry air whose concentration was regulated through a needle valve. Radiations from the axial region of positive column of the diffuse arc discharge were focussed by lens arrangements on the slit (of width 0.5 mm.) of an accurately calibrated constant deviation spectrograph.

The triplet radiations: 5461 Å ($7^3S_1 \longrightarrow 6^3P_2$), 4358 Å ($7^3S_1 \longrightarrow 6^3P_1$) and 4047 Å ($7^3S_1 \longrightarrow 6^3P_0$) were focussed seperately on the cathode of a photomultiplier (M10 FS29V λ). Details of electronic arrangements for measuring the intensities of spectral lines are given in Chapter II.

In the present investigation, the arc current was varied between 2 to 3 amps., pressure of air was varied from 0.05 torr to 1 torr. and temperature of the inner wall of discharge tube T_W was observed to vary between 98°C to 115°C.

7.3. Results and discussions

The triplet radiations ($7^3S_1 \longrightarrow 6^3P_{0,1,2}$) escaping from the axial region of positive column of a low pressure mercury arc discharge are observed to be enhanced in presence of a longitudinal magnetic field (0-1500 gauss). The ratio I_B/I, where I_B and I are the intensities of radiation when a magnetic field is present and not, increases, thereafter passing through a broad maxima, very slowly decreases. Fig. 7.1, shows the variation of I_B/I with B when the discharge current is 2 amp. and pressure of air inside the discharge tube is 0.05 torr. It is observed that $(I_B/I)_{max.}$ values are different for three lines. The 4047 Å line ratio increases rather rapidly and reaches the broad maxima in comparatively low magnetic field. For other two lines I_B/I reaches

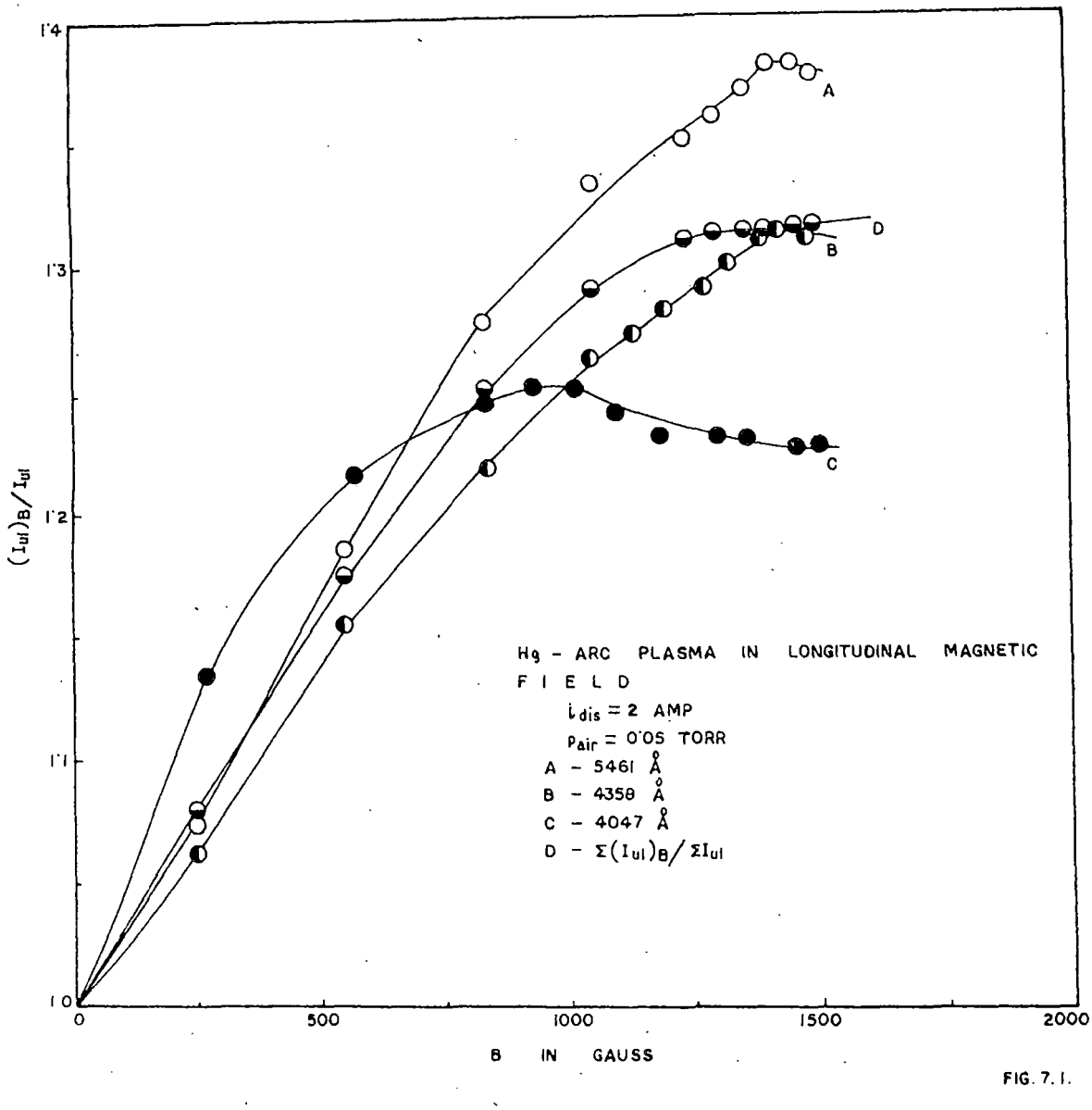

Fig. 7.1. Variation of spectral intensity enhancement factors (I_B/I) with longitudinal magnetic field for lines originating from 7^3S_1 level of mercury, i = 2A.

its maximum value nearly in the same field. The nature of the curves remains same when the discharge current was varied from 2 to 3 amps. and pressure of air inside the discharge tube was changed from 0.05 torr to 1 torr. F Fig. 7.2 shows a plot of I_B/I Vs. B when the discharge current is 2.25 amp. and p_{air} is 0.9 torr.

For a comparison of the effect of a longitudinal magnetic field to that of a transverse magnetic field the measured values of radiation enhancements (I_B/I) for different values of transverse magnetic field has been plotted in Fig. 7.3.

Table 7.1 shows the values of B_{max} when the enhancement maxima occurs along with the values of $(I_B/I)_{max}$ for the three lines considered for different discharge conditions.

In chapter III it was observed that when a discharge column was subjected to a magnetic field there occured a coupled variation of axial electron density $n_e(0)$ and electron temperature T_e. (T_e is assumed to be uniform along the cross section of discharge tube). In the case of a longitudinal magnetic field $n_e(0)$ increases and T_e decreases, whereas when the magnetic field is transverse to the direction of current, $n_e(0)$ decreases and T_e increases with the increase of magnetic field. In the latter case, the cylindrical symmetry of the plasma column is shifted towards the wall in the direction

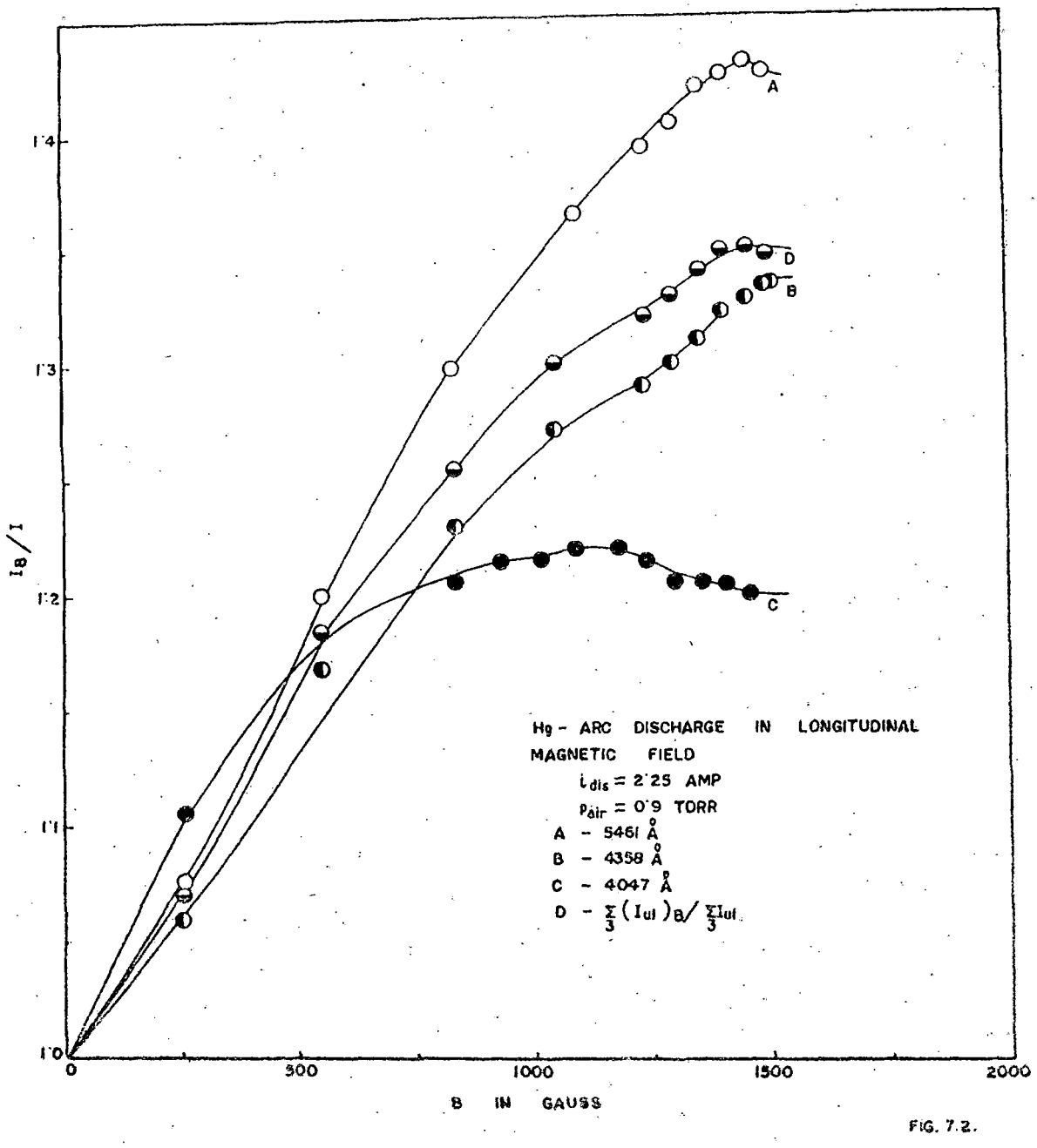

Fig. 7.2. Variation of spectral intensity enhancement factors (I_B/I) with longitudinal magnetic field for lines originating from 7^3S_1 level of mercury, i = 2.5A.

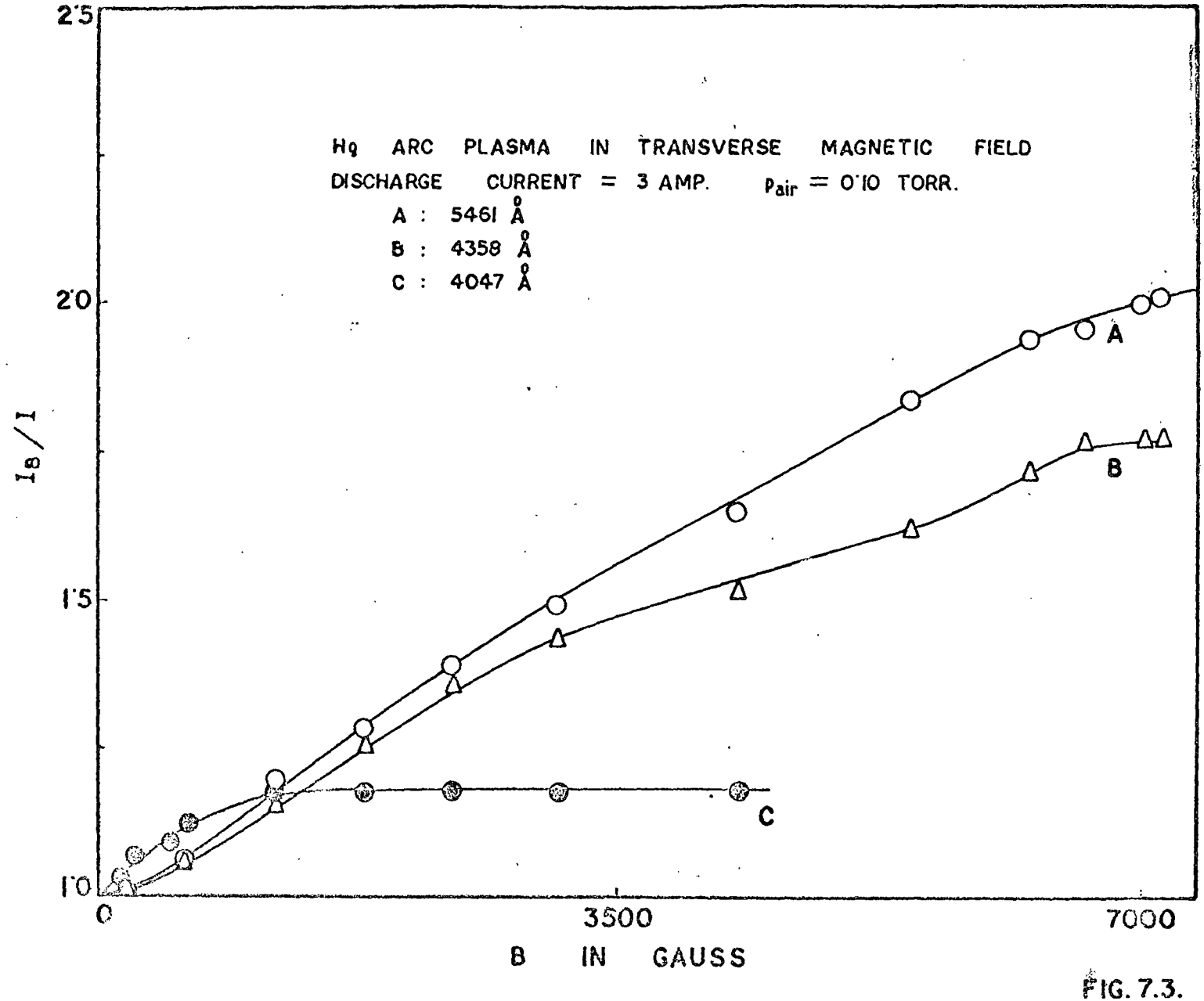

FIG. 7.3.

Fig. 7.3. Variation of spectral intensity enhancement factors with transverse magnetic field for mercury arc.

TABLE 7.1

Wavelength (Å)	Values of B_{max} and $(I_B/I)_{max}$	p_{air} = 0.5 torr.		p_{air} = 0.9 torr.	
		i = 3A	i = 2A	i = 2.25 A	i = 2.75 A
5461	B_{max}	1405 G	1405 G	1455 G	1455 G
	$(I_B/I)_{max}$	1.312	1.38	1.43	1.46
4358	B_{max}	1455 G	1425 G	1495 G	1455 G
	$(I_B/I)_{max}$	1.275	1.316	1.332	1.33
4047	B_{max}	1015 G	930 G	1055 G	1015 G
	$(I_B/I)_{max}$	1.25	1.25	1.22	1.23

of Lorentz force. Spectral enhancement is dependent f on n_e (0) and T_e. Since all the three lines originate from a single upper level (7^3S_1), their dependence on $n_e(0)$ and T_e will be same resulting in same rate of radiation enhancement for the three lines. Since this is not the case in reality, it may be concluded that a third factor which is different for three lines, is important in the process of radiation enhancement. Les' et al (1961) have observed that intensity ratios of the visible triplets of mercury atoms

differ widely depending upon the condition of source. All these divergences can be explained by the phenomena of re-absorption of lines. The lower levels of the lines are two metastables ($6^3P_{0,2}$) and a resonance (6^3P_1) level. In the steady state they are supposed to build up appreciable populations, thereby causing self absorption of the lines. As self absorption affects the intensity of emission lines and is strongly related to the population of lower levels, the enhancement factor will also depend on population densities of lower levels of the lines. In the next section a quantitative estimate of this effect has been discussed.

7.3.1. Self absorption and enhancement factors in magnetic field:

When there is appreciable self absorption, spectral intensity I_{ul} of a line with upper level u and lower level l is given as,

$$I_{ul} = \text{const.}\, A_{ul} \int_{-R}^{R} n_u(r) \left[\int_{-\infty}^{\infty} \alpha(\nu) \exp\left(-\beta(\nu)\sigma \int_{r}^{R} n_l(r)\, dr\right) d\nu \right] dr \qquad (7.1)$$

where $n_{u,l}(r)$ are the local number densities of the upper radiating level and the lower level as a function

of position r along the line of sight. A_{ul} is the transition probability of the line and $\alpha(\nu)$ is the normalised spectral emission profile $\int \alpha(\nu)\, d\nu = 1$

The fraction of emitted line which reaches the detector after traversing the medium from position r is

$$\exp.\left(-\sigma \beta(\nu) \int_{r}^{R} n_l(r)\, dr\right)$$

σ is the absorption cross section per atom at the line centre, independent of r and $\beta(\nu)$ is the line profile of absorption normalised to unity at the line centre $\beta(\nu_0) = 1$, and $r = 0$ at the centre of the discharge.

When there is no self absorption

$$I_{ul}^{o} = \text{const.}\ A_{ul} \int_{-R}^{R} n_u(r) \left[\int_{-\infty}^{\infty} \alpha(\nu)\, d\nu\right] dr$$

$$= \text{const.}\ A_{ul} \int_{-R}^{R} n_u(r)\, dr \qquad (7.2)$$

Vriens et al (1978) and Uvarov and Fabrikant (1965) have shown that excited mercury atoms distribution function across the cross section of discharge is nearly parabolic. Thus considering a parabolic distribution of $n_u(r)$ we get

$$I_{ul}^{o} = \text{const.}\ A_{ul}\, \frac{4}{3}\, n_u(0)\, R \qquad (7.3)$$

Here $n_u(0)$ is the number density of radiating atoms at the axis of the discharge tube.

Now self absorption As of a spectral line is defined as

$$I_{ul} = (1 - A_s)\, I^{\circ}_{ul}$$

$$= \text{const.}\,(1 - A_s)\, n_u(0)\, A_{ul} \qquad (7.4)$$

when a longitudinal magnetic field B is present

$$(I_{ul})_B = \text{const.}\,(1 - A_s)_B\, n_u(0)_B\, A_{ul} \qquad (7.5)$$

From (7.4) and (7.5) we get,

$$\frac{(I_{ul})_B}{I_{ul}} = \frac{(1 - A_s)_B}{1 - A_s}\ \frac{n_u(0)_B}{n_u(0)} \qquad (7.6)$$

If both the upper and lower level population densities are parabolic

$$n_x(r) = n_x(0)\left(1 - \frac{r^2}{R^2}\right)$$

we are assuming that source is of type 'uniform excitation' i.e. a source in which the radiating and absorbing atoms are distributed in the same manner.

Now,

$$1 - A_s = \frac{I_{ul}}{I_{ul}^{o}}$$

$$= \left(\int_{-R}^{R} n_u(r) \left[\int_{-\alpha}^{\alpha} \alpha(\nu) \exp\left(-\beta(\nu)\sigma \int_{r}^{R} n_\ell(r)\,dr\right) d\nu \right] dr \right) \Big/ \frac{4}{3} R\, n_u(0) \qquad (7.7)$$

We first decouple the integrals over $n_u(r)$ and $n_\ell(r)$

$$\sigma \int_{r}^{R} n_\ell(r)\,dr = \sigma R \int_{y}^{1} n_\ell(0)\,(1-y^2)\,dy$$

$$= \sigma R\, n_\ell(0) \left[\frac{2}{3} - y\left(1 - \frac{y^2}{3}\right) \right]$$

where $y = r/R$

putting this value in third bracket of R.H.S. of eqn.(7.7) and replacing the exponential by its power series,

$$\int_{-\alpha}^{\alpha} \alpha(\nu) \exp\left(-\beta(\nu)\sigma R\, n_\ell(0) \left[\frac{2}{3} - y\left(1 - \frac{y^2}{3}\right) \right]\right) d\nu$$

$$= \int_{-\alpha}^{\alpha} \alpha(\nu) \sum_{n=0}^{\infty} \frac{(-1)^n R^n \sigma^n \beta^n(\nu)}{n!}\, n_\ell(0)^n \left[\frac{2}{3} - \left(y - \frac{y^3}{3}\right) \right]^n d\nu$$

$$= \sum_{n=0}^{\infty} \frac{(-1)^n R^n \sigma^n n_\ell(0)^n}{n!} \left[\frac{2}{3} - \left(y - \frac{y^3}{3}\right) \right]^n \int_{-\alpha}^{\alpha} \alpha(\nu)\, \beta^n(\nu)\, d\nu$$

For a discharge type like ours we can safely assume that emission and absorption profiles are identical and Gaussian in nature which is the outcome for Doppler broadening of spectral lines. That is we assume all other broadenings of the spectral lines negligible compared to Doppler broadening. Validity of these criterions is discussed in text books (Corney, 1977) and for resonance line by Hearn (1963). For a Gaussian profile of absorption and emission, Mosberg and Wilke[i] (1978) have shown

$$\int_{-\infty}^{\infty} \alpha(\nu)\,\beta^{n}(\nu)\,d\nu = \frac{1}{n+1}$$

Putting all these results in (7.7) we obtain

$$1 - A_s = 1 - \frac{3}{4}\sum_{n=1}^{\infty} \frac{(-1)^{n+1}\sigma^{n} n_e(0)^{n} R^{n}}{n!\,(n+1)} \int_{-1}^{+1} \left[\frac{2}{3} - \left(y - \frac{y^3}{3}\right)\right]^{n} (1-y^2)\,dy$$

or,

$$1 - A_s = 1 - \frac{3}{4}\sum_{n=1}^{\infty} \frac{(-1)^{n+1}\sigma^{n} n_e(0)^{n} R^{n}}{(n+1)!} \left[\int_{-2/3}^{+2/3} \left[\frac{2}{3} - \left(y - \frac{y^3}{3}\right)\right]^{n} d\left(y - \frac{y^3}{3}\right)\right] \qquad (7.8)$$

values of $n_e(0)$'s are calculated by employing Forrest and Franklin's (1969) equation in a fashion stated in chapter VI. To determine the value of $n_0(0)$, $n_1(0)$ and $n_2(0)$ the population densities of $6^3P_{0,1,2}$

levels at the axis of the discharge, we have utilised the values of collision integrals $\langle Q_{ij}\vartheta \rangle$ given by Johnson, Cooke and Allen (1978) (author's Fig. No. 7 and reproduced in fig. 7.4). A survey of literature revealed a large range of cross section (Q_{ij}) values. From these large datas the authors have chosen a set which appears self consistent and in which the forward and reverse rates are related by Klein-Rosseland formula. The density of electron at the axis n_e (0) without a magnetic field is determined from the expression of current considering a parabolic distribution of electron.

$$i = \mu E e 2\pi \int_0^R n_e(r) r\, dr$$

$$= \mu E e 2\pi n_e(0) R^2 \int_0^1 y(1-y^2)\, dy$$

where μE is the drift velocity of electrons in mercury vapour at the corresponding E/p determined by Nakamura and Lucas (1978). This value of $n_e(0)$ was utilised in the calculations of population densities in a manner stated in chapter VI.

For a discharge with a Maxwellian electron energy distribution function and for current i = 2.5 amp., p_{air} = 0.5 torr and p_{Hg} = 0.2729 torr determined by inner

Fig. 7.4. Collision integrals $\langle Q_{ij}\, v \rangle$ for Hg. levels: (a) inelastic with ground state, (b) inelastic with 6^3P levels; (c) super-elastic. A, $6^1S_0 \rightleftharpoons 6^3P_0$, B, $6^1S_0 \rightleftharpoons 6^3P_1$, C, $6^1S_0 \rightleftharpoons 6^3P_2$, D, $6^3P_0 \rightleftharpoons 6^3P_1$, E, $6^3P_1 \rightleftharpoons 6^3P_2$.

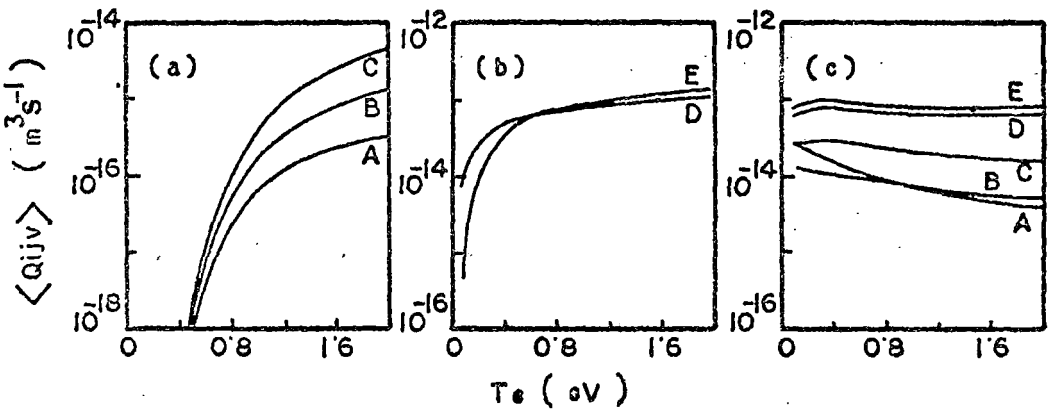

FIG. 7.4.

wall temperature T_g, and T_e = 0.412 eV. as determined by spectral intensity ratio method in chapter VI, the result of calculations is: n_g (considered uniform across c.s.) = 9.6×10^{15} cm^{-3}, $n_e(0)$

$$= 5.95 \times 10^{13} \text{ cm}^{-3}.$$

$$n_2(0) = 1.13 \times 10^{10} \text{ cm}^{-3}$$

$$n_1(0) = 2.38 \times 10^{10} \text{ cm}^{-3}$$

$$n_0(0) = 3.92 \times 10^{10} \text{ cm}^{-3}$$

Again σ the cross section of absorption at the line centre, when Doppler broadening is the sole broadening mechanism of spectral lines, is given as

$$\sigma = \pi r_0 c f_{lu} \lambda_{ul} \left(\frac{M}{2\pi k T_g}\right)^{1/2} \qquad (7.9)$$

where r_0 is the classical electron radius, (2.818×10^{-13} cm). c is the velocity of light, f and λ are the absorption oscillator strength and wavelength of the transition, M is the mass of mercury atom and k is the Boltzmann constant. Taking f values of the transitions from Gruzdev (1967), the calculated value of σ by equation (7.9) and the values of $k_0 = \sigma n_l(0)$ where k_0 is the absorption coefficient of radiation at the line centre has been shown in Table 7.2.

TABLE 7.2

λ (Å)	5461	4358	4047
f (Ref. Gruzdev (1967))	0.14	0.11	0.10
σ (cm^2)	6.5×10^{-12}	4.077×10^{-12}	3.44×10^{-12}
k_o (cm^{-1})	0.0735	0.0938	0.1348

It is evident from Table 7.2 that k_oR, ($R = 0.75$ cm.) which may be called the optical depth is much smaller than unity. Since the series in eqn. (7.8) is a converging one we discard all the terms except the first term $n = 1$.

Thus

$$1 - A_s = 1 - \frac{3}{4}\sigma n_\ell(0) R \frac{1}{2}\left[\frac{8}{9}\right]$$

or, $$1 - As = 1 - \frac{1}{3}\sigma n_\ell(0) R$$

$$= 1 - f_{\ell u} \lambda_{u\ell} \rho n_\ell(0) \qquad (7.9)$$

where $$\rho = \frac{1}{3}\pi r_o C \left(\frac{M}{2\pi k T_g}\right)^{1/2} R$$

Putting the value of $(1 - As)$ from eqn. (7.9) in eqn. (7.6)

we obtain,

$$\frac{(I_{ul})_B}{I_{ul}} = \frac{1 - f_{lu}\lambda_{ul}\rho\, n_l(0)_B}{1 - f_{lu}\lambda_{ul}\rho\, n_l(0)} \frac{n_u(0)_B}{n_u(0)}$$

We have assumed here that neutral atom temperature is constant with magnetic field though we were unable, to measure the change of T_g with B experimentally. Hence

$$(I_{ul})_B / I_{ul} = \left[1 - f_{lu}\lambda_{ul}\rho\left(n_l(0)_B - n_l(0)\right)\right] \frac{n_u(0)_B}{n_u(0)} \qquad (7.10)$$

Due to coupled change of $n_e(0)$ and T_e with magnetic field, $n_u(0)$ and $n_l(0)$ will change. Equation (7.10) qualitatively predicts that due to these changes enhancement of spectral radiations will also change but will be lessened by self absorption as $n_l(0)$ increases with B. The effects will be different for three lines as f, λ and $n_l(0)_B$ will be different for them. It may be noted here that σ is maximum for 5461 Å radiation where as $n_2(0)$ is relatively small. The case is reversed for 4047 Å radiation, the case for 4347 Å radiation is in between them.

Moreover, measurement of T_e with B in chapter VI (fig. 6.2) shows that as B increases, T_e decreases and reaches a saturated lower value. The case is

reversed for $n_e(0)$. Anyway it may be concluded that due to coupled change of $n_e(0)$ and T_e with B both $n_\ell(0)$ and $n_u(0)$ will attain a saturated upper value. Moreover, it is established that for a source of uniform excitation, there will be no self-reversal (Cowan and Diecke (1948)), on the other hand effect due to self absorption will also reach a saturated maximum value. Thus we can expect that when B is sufficiently large there will be no change in enhancement factor with the increase of magnetic field. Fig. 7.1 and 7.2 however shows a slow fall of the factor at that stage.

Now we consider a discharge in sufficiently high magnetic field (as B = 1500 gauss), so that all changes are saturated. In that case $n_\ell(0)_B >> n_\ell(0)$ Since relative populations of the excited levels always obey a Boltzmann distribution with T_e as temperature (Richter, 1968), eqn. (7.10) may be re-written as

$$\frac{(I_{ul})_{max}}{I_{ul}} = \left[1 - f_{\ell u}\lambda_{ul} P n_0(0)_B \exp\left(-\frac{E_\ell - E_0}{kT_{eB}}\right)\right]\frac{n_u(0)_B}{n_u(0)} \qquad (\ell = 0, 1, 2) \qquad (7.11)$$

here $E's$ are the energy of the corresponding levels. In the L.H.S. of eqn. (7.11) we have written the subscript

max indicating that the saturation maxima has been reached. For 4047 Å, for which the maxima is attained earlier, we consider that this is also the value for I_B when B is much greater than B_{max} where the intensity maximum was first attained.

A plot of $(I_{ul})_{max} / I_{ul}$ against

$$f_{lu} \lambda_{ul} \exp(-(E_l - E_o)/kT_{eB})$$

has been shown in Fig. 7.5 for two discharge conditions, and the plots are straight lines as predicted by eqn. (7.11). The slope of the lines are :

i) for i = 2 amp., p_{air} = 0.05 torr, slope 3.33 x 10^4 cm^{-1}.

ii) for i = 2.25 amp., p_{air} = 0.9 torr, slope = 5.19 x 10^4 cm^{-1}. The slope = $\frac{1}{3} \pi r_o c R \times (M/2\pi k T_g)^{1/2} n_o(0)_B \, n_u(0)_B / n_u(0)$

From the intercept of the graph $n_u(0)_B / n_u(0) \approx 1 \cdot 4$

if $n_o(0)_B \approx 10 \times$ magnitude of $n_o(0)$

$\approx 10^{11}$ cm^{-3}

the calculated value of slope is,

$$(\text{slope})_{\text{calculated}} = \frac{1}{3} \times 3{\cdot}14 \times 2{\cdot}82 \times 10^{-13} \times 3 \times 10^{10} \times 0{\cdot}75 \times 10^{11} \times 1{\cdot}4 \times \left(\frac{200 \times 1{\cdot}66 \times 10^{-24}}{2 \times 3{\cdot}14 \times 1{\cdot}38 \times 10^{-16} \times 373} \right)^{1/2}$$

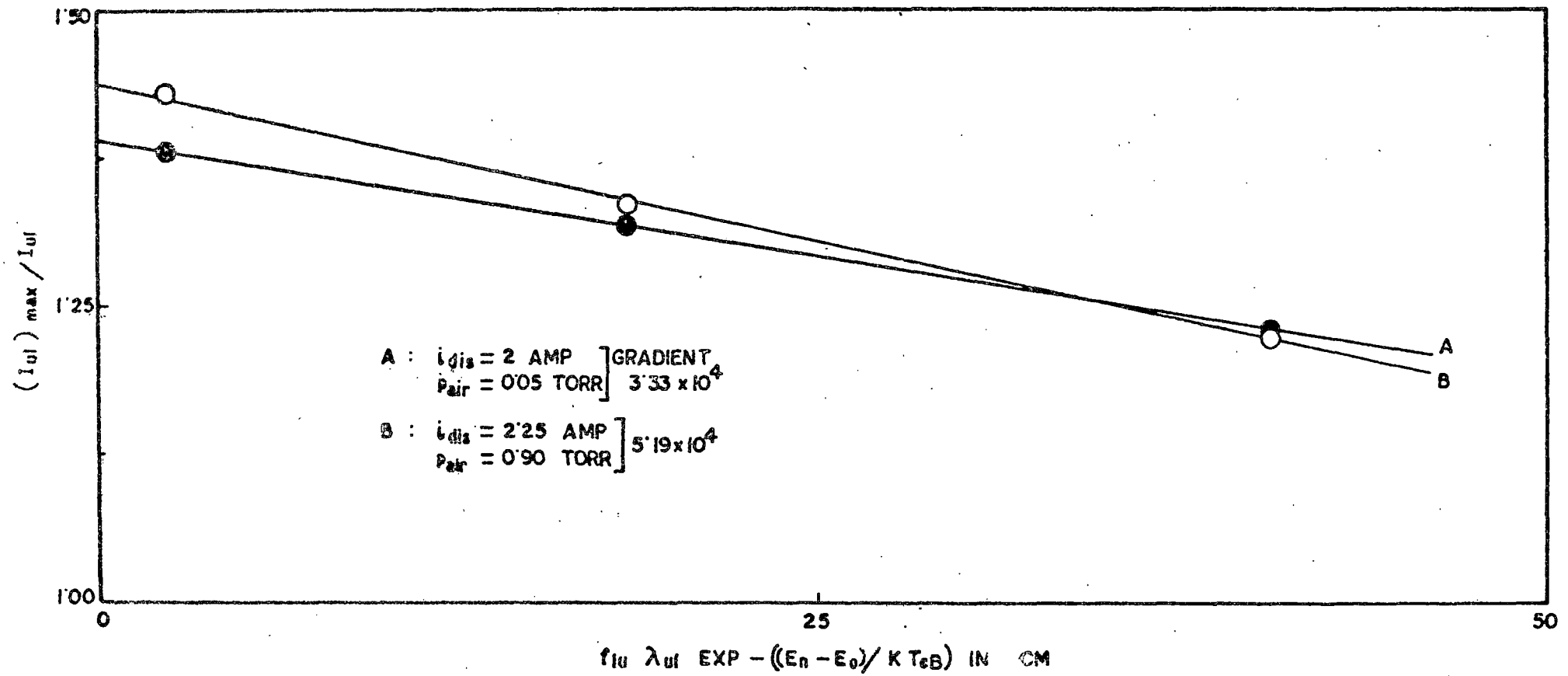

Fig. 7.5. Variation of enhancement maxima against $f_{lu}\lambda_{ul}\exp\left[-(E_n-E_o)/kT_{eB}\right]$ for two types of mercury arc discharges in longitudinal magnetic field.

$\approx 3 \times 10^4$ cm^{-1} which is in agreement with the values determined from graph.

In the next sections we shall try to evaluate the value of $n_i(0)_B / n_i(0)$ from the total intensity of the triplet lines. Before doing this we shall consider the positive column of mercury arc discharge in detail so that the coupled variation of T_e and $n_e(0)$ may be predicted and this has been shown in the following section.

7.3.2. Coupled variation of $n_e(0)$ and T_e with magnetic field :

We shall consider a wall confined diffuse mercury arc discharge the type of which was discussed indetail in chapter VI. It was observed there that chief ionised species are Hg_2^+ molecular ions formed by the process of associative ionisation when p_{air} is relatively small and when p_{air} is relatively high (> 2 torr.) due to quenching of 6^3P_0 and 6^3P_1 levels by N_2 and O_2 molecules, Hg^+ ions, created by electron collision of 6^3P_2 level atoms, are the chief ionised species. When p_{air} is relatively small, Hg_2^+ molecular ions are formed by reactions like

$$Hg(6^3P_0) + Hg(6^3P_1) \rightarrow Hg_2^+(6^2\Sigma^+) + e$$

this process has a large cross-section. If we consider that the axial neutral particle temperature of the arc is larger than the inner wall temperature, which is generally the case as an appreciable amount of energy which is supplied to the arc is carried away by the thermal conductivity of mercury vapour atoms and air molecules, the rate of production of Hg_2^+ ions will further increase than as calculated in chapter VI. For a group of processes like

$$Hg\,(6^3P_1) + Hg\,(6^3P_2) \rightarrow Hg^* + Hg\,(6^1S_0)$$

$$Hg^* + e \rightarrow Hg^+ + 2e$$

the Hg* states are highly excited states and are very near to the ionisation level. These levels are definitely in thermal equilibrium with the free electrons. Principle of detailed balancing predicts an equal downward collision of Hg* atoms with Hg (6^1S_0) atoms to form 6^3P_1 and 6^3P_2 atoms instead of reaction like $Hg^* + e \rightarrow Hg^+ + 2e$. Hence one of the chief Hg^+ ion production mechanism can not be considered as Hg* atoms are in thermal equilibrium with continuum, rendering the ionic species of the discharge more molecular.

Thus we consider a positive column of discharge where Hg_2^+ ions are produced by the process of associative ionisation and lost by ambipolar diffusion to the wall.

We neglect the effect of conversion of molecular ions to atomic ions and vice-mersa and the process of dissociative recombination of molecular ions. Ignoring the radial variation of 6^3P_0 atoms, the equation of continuity for electron is

$$\frac{1}{r}\frac{d}{dr}\left(r\frac{dn_e(r)}{dr}\right) = -\frac{g}{D_a} \qquad (7.12)$$

where $g = n_o n_1 \sigma_{ass} \langle v \rangle$, σ_{ass} = c.s. for associative ionisation and $\langle v \rangle = (16kT_g/\pi M)^{1/2}$ and Da is ambipolar diffusion coefficient. The solution of (7.12) with $n_e(R) = 0$ at the wall is

$$n_e(r) = \frac{gR^2}{4D_a}\left[1 - \left(\frac{r}{R}\right)^2\right] \qquad (7.13)$$

Since $D_a = \mu_i kT_e/e$ where μ_i is the mobility of Hg_2^+ ions, the plasma balance condition is obtained

$$\frac{gR^2}{n_e(0)\mu_i kT_e/e} = 4 \qquad (7.14)$$

It may be noted here that for a parabolic profile of $6^3P_{0,1}$ atoms the eqn. (7.13) changes to

$$n_e(r) = \frac{gR^2}{4D_a}\left[\frac{11}{72} - \frac{1}{4}\left(\frac{r}{R}\right)^2 + \frac{1}{8}\left(\frac{r}{R}\right)^4 - \frac{1}{36}\left(\frac{r}{R}\right)^6\right]$$

but eqn. (7.14) virtually remains unchanged only 72/11 replacing 4 in the R.H.S.

Since the conditions for ions to be magnetised is $B/p > 0.5$ tesla torr^{-1} (Franklin, 1976), we consider for our experimental conditions $\mu_i = \mu_{iB}$, more over it was observed by Cummings and Tonks (1941) that normal distribution of electrons is characteristic of an arc in its steady state even in presence of a longitudinal magnetic field, the plasma balance equation in the presence of a magnetic field will be

$$\frac{g_B R^2}{n_e(0)_B \mu_i k T_{eB}/e} = 4 \qquad (7.15)$$

the subscript B signifies the corresponding quantities when a magnetic field is present. From (7.14) and (7.15) we get

$$\frac{n_e(0)_B}{n_e(0)} \cdot \frac{kT_{eB}}{kT_e} = \frac{g_B}{g} \qquad (7.16)$$

The ratio g_B/g is again a function of $n_e(0)$ and T_e. This functional relationship may be estimated very approximately in the following manner:

6^3P_0 and 6^3P_1 level populations which enter into g are a metastable and resonance level. In the steady state, they are supposed to build up appreciable

populations and collisional processes chiefly populate and depopulate the levels. Let us assume that they build up an equilibrium population distribution as determined by Saha equation

$$[n_o(0)]_{\text{equilibrium}} = \frac{g_o}{2g_i}\left(\frac{2\pi\hbar^2}{mkT_e}\right)^{3/2} n_e(0)^2 \exp\left(\chi_o / kT_e\right) \qquad (7.17)$$

here g_o and g_i's are the statistical weights of 6^3P_0 state and atomic ions, χ_o is the ionisation potential of 6^3P_0 state, m equals the mass of electron and $\hbar$ is the rationalised Plank's constant, $n_e(0)$ here is the density of Hg^+ ions which may be roughly calculated knowing T_e and n_g by Saha equation and was calculated as 1.78×10^{13} cm^{-3}. Now for a level to be in thermal equilibrium microreversibilities would have to exist for all processes. In this way, one of the processes say electron impact ionisation of 6^3P_0 atoms should be balanced by three body collisional recombination of atomic ions with electrons to that level. But unfortunately for discharges under consideration, this is not the case. Microreversibilities for ionisation process are totally absent. Instead, the ions produced in the volume are carried away to discharge tube wall by

irreversible ambipolar diffusion process, thereby they recombine at the wall and return to the plasma region as neutral ground state species. This is also equally true for molecular ions. Molecular ions do not recombine totally in the volume, instead a large amount of excess of ions are carried away towards the wall by ambipolar diffusion. In short in these types of plasma, ionisation does not balance with recombination. This type of discharges are named as 'ionising plasma' by Fujimoto (1979). In this case, following Numano et al (1975) we can write,

$$n_o(0) = (1+C_p)\left[n_o(0)\right]_{\text{equilibrium}} \quad (7.18)$$

Here C_p is a quantity which determines the excess of ionisation over volume recombination and C_p is given as (approximately)

$$C_p = 10^{31}\frac{D_a}{n_e(0)^2\Lambda^2}\left(\frac{E_H}{kTe}\right)^{1/2}\frac{1}{g_o g_{etb}^s}\exp\left(-\frac{\chi_i'}{kTe}\right) \quad (7.19)$$

here Λ is the effective diffusion length and $1/\Lambda^2 = (2.4/R)^2$, E_H is the ionisation potential of hydrogen atoms, χ_i' being the ionisation potential of the lowest excited state, in the case of mercury

atoms $\chi_i' = \chi_o$ and q_{eff} is identified as effective quantum no. of the state defined as (Griem,1964),

$$q_{eff} = z\left(\frac{R}{T_\alpha - T_p}\right)^{1/2}$$

where R = Rydberg constant, T_α is the ionisation limit of the system under consideration, T_p is the term value of the x level p and for neutral atoms Z = 1.

Nishikawa et al (1971) have determined the value of $D_a = 160/p$ $cm^2 sec^{-1}$, with this value of D_a and $n_e(0) = 1.78 \times 10^{13}$ cm^{-3} determined by Saha equation, the value of C_p is found to be 28.85. Since $C_p >> 1$, we rewrite equation (7.18) as

$$n_o(0) = \delta\left(\frac{1}{kT_e}\right)^2 D_a \qquad (7.20)$$

where $$\delta = 10^{31}\frac{1}{\Lambda^2}(E_H)^{1/2}\frac{1}{2g_i q_{eff}^8}\left(\frac{2\pi\hbar^2}{m}\right)^{3/2}$$

Again considering $D_a = \mu_i kT_e/e$

we arrive at the conclusion

$$n_o(0) \propto \frac{1}{kT_e} \qquad (7.21)$$

This result is also evident from the generalised expression for electron temperature (von-Engel, 1965) in which it has been shown that $T_e \propto (E/p)$ where p is

the pressure which is a measure of $n_o(0)$.

Since relative populations of excited states obey Boltzman distribution we can write also,

$$n_1(0) \propto \frac{1}{kT_e} \qquad (7.22)$$

Here we have neglected the exponential term since

$$kT_e > \Delta E$$

It may be noted here that the proportionality constants in (7.21) and (7.22) would be independent of magnetic field, so long B/p is less than the limit for which ions remain un-magnetised.

So eqn. (7.16) may be rewritten as

$$\frac{n_e(0)_B}{n_e(0)} = \left(\frac{kT_e}{kT_{eB}}\right)^3 \qquad (7.23)$$

Here we have assumed once again that

$$T_g = T_{gB}$$

As measured values of T_e in chapter VI, show a decrease with the increase of B, equation (7.23) predicts a coupled increase of $n_e(0)$ with B though very approximately. However, we have plotted T_{eB} / T_e and $n_e(0)_B / n_e(0)$ with B in Fig. 7.6. This relationship (7.23) will be utilised in next section while determining the population density of 6^3P_2 level from total intensity of triplet lines.

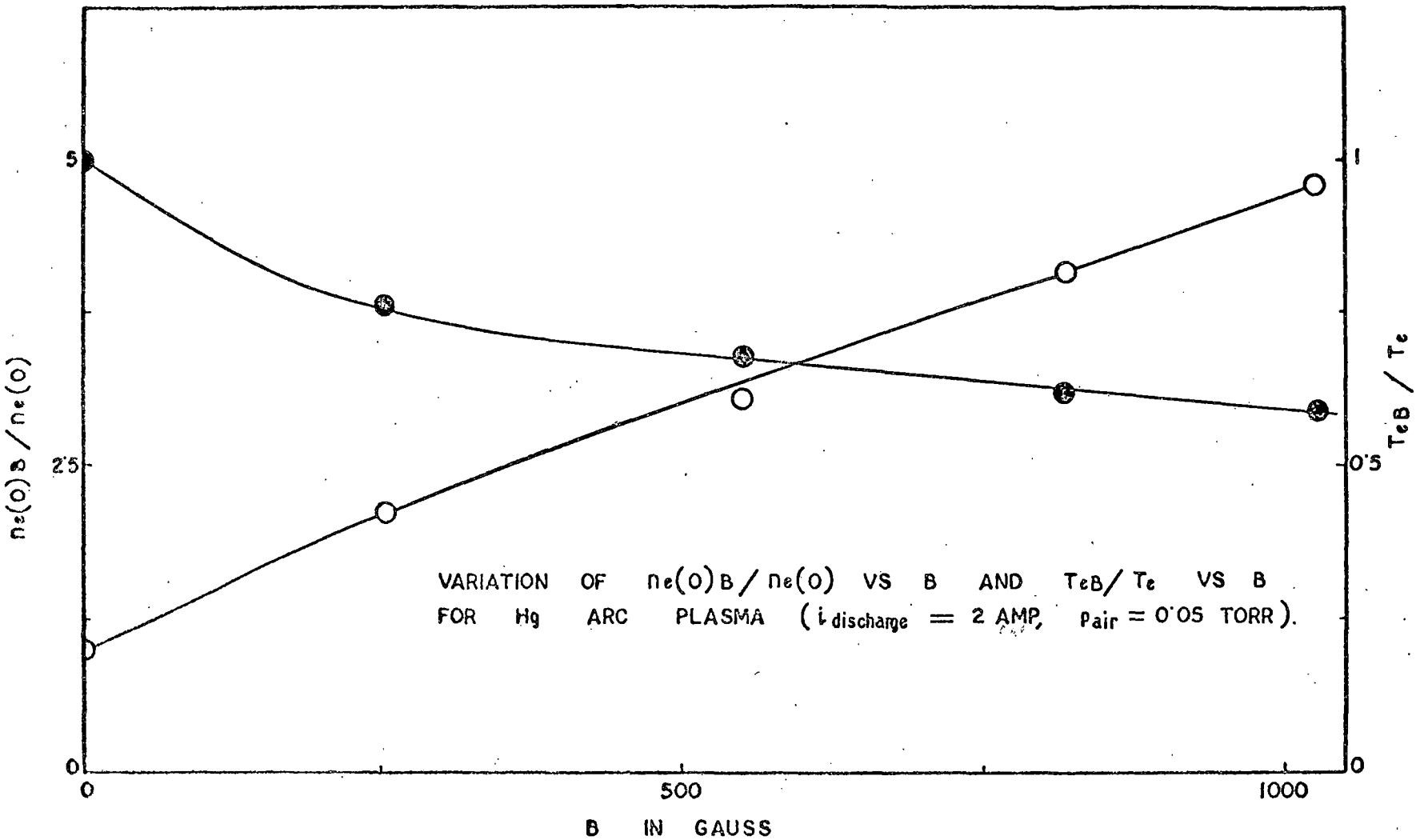
5
2·5
0
0
500
1000
B IN GAUSS
ne(0)B / ne(0)
TeB / Te
1
0·5
0
VARIATION OF ne(0)B / ne(0) VS B AND TeB / Te VS B
FOR Hg ARC PLASMA (i discharge = 2 AMP, Pair = 0·05 TORR).

FIG. 7.6.

7.3.3. Total intensity of triplet lines with and without magnetic field.

For a homogeneous and isotropic source, the intensity of a spectral line is given as,

$$I_{ul} = \frac{h\nu_{ul}}{4\pi} A_{ul}\, \theta_{ul} \int n_u(r)\, dr \qquad (7.24)$$

where θ_{ul} is the optical escape factor which accounts for the self absorption of the line.

Thus for the three lines considered together,

$$\frac{\sum_3 (I_{ul})_B}{\sum_3 (I_{ul})} = \left(\sum A_{ul}\, \theta_{ul}\right)_B \frac{n_u(0)_B}{n_u(0)} \cdot \frac{1}{\sum A_{ul}\, \theta_{ul}} \qquad (7.25)$$

Here $n_u(0)$ represents the axial density of 7^3S_1 atoms. To determine $n_u(0)$, we shall consider the production and loss mechanism of 7^3S_1 atoms.

The level 7^3S_1 may be populated by one or more of the following ways:

i) direct excitation of the ground level atoms.

ii) stepwise excitation of $6^3P_{0,1,2}$ levels.

iii) cascade radiations chiefly from 7^3P_2 level.

iv) transfer of excitation by electron collision from other higher levels.

v) bi-molecular excited dimmer collision followed by a decomposition to 7^3S_1 level.

(a) $Hg_2^* + Hg_2^* \rightarrow Hg_2^{**} + 2\,Hg$

(b) $Hg_2^{**} \rightarrow Hg\ (6^1S_0) + Hg^*\ (7^3S_1)$

vi) recombination of Hg^+ ions to the x level.

The level may be depopulated by one or more of the following processes:

i) spontaneous emission.

ii) collisional de-excitation to a lower level.

iii) collisional excitation to a higher level.

iv) ionisation from the level.

v) quenching by N_2 and O_2 molecules.

Now let us consider the relative importance of production and loss terms. In the production side contribution due to processes (iv), (v) and (vi) may be neglected in our conditions of discharge. We also disregard cascade contribution to 7^3S_1 level as the electron temperature is small enough rendering population in 7^3P levels small. So the important terms will be direct and stepwise excitations. Again it is evident that contribution of stepwise excitations from 6^3P_2 level will dominate over that for other levels $6^3P_{0,1}$. We have calculated the rate of this excitation corresponding to a optically allowed transition by M.J.Seaton's

cross section (Sampson, 1969) and rate of ($6^1S_0 \rightarrow 7^3S_1$) from the ground state which is a optically forbidden transition by C.W.Allen's cross section (Benson and Kulander, 1972). The calculated values of the rates are

rate for ($6^1S_0 \longrightarrow 7^3S_1$) transition = $2.69 \times 10^{13} sec^{-1}$

rate for ($6^3P_2 \longrightarrow 7^3S_1$) transition = $1.4 \times 10^{14} sec^{-1}$

i.e. stepwise excitation is nearly a magnitude greater than the direct excitation.

In the loss side collisional excitation to the nearest higher level 7^1S_0 (7.926 eV.) will be dominating to that for all other higher levels and collisional excitation to a higher level will be greater than collisional de-excitation to a lower level. Hence comparable terms will be spontaneous emission lessened by self absorption and collisional excitation to 7^1S_0 level. Self absorption of a transition is accounted for by introducing escape factor parameter θ_{ul} which is given by a relation deduced by Phelps et al (1960, 1958),

$$\theta_{ul} = \frac{1.92 - \dfrac{1.3}{1+(k_0R)^{6/5}}}{(k_0R+0.62)\left\{\pi \ln(1.375+k_0R)\right\}^{1/2}} \qquad (7.26)$$

The transition probabilities A_{ul} for three lines for 7^3S_1 level are given by Mosberg & Wilkie (1978). With these values of A_{ul} and θ_{ul} calculated by

equation (7.26) with values of k_o given in table 7.2, we calculate contribution for spontaneous emission

$$n_u(0) \sum A_{ul} \theta_{ul} = 6.77 \times 10^8 n_u(0) \quad sec^{-1}$$

The contribution of optically forbidden transition $(7^3S_1 \rightarrow 7^1S_0)$ is 3.23×10^6 $n_u(0)$ sec^{-1}, whereas the rate of quenching of 7^3S_1 atoms by N_2 and O_2 molecules will be in the order 10^4 $n_u(0)$ sec^{-1}, the cross sections for quenching collisions are given by Massey (1971). Thus we arrive at the balance equation for 7^3S_1 atoms

$$n_u(0) \sum A_{ul} \theta_{ul} = n_e(0) n_2(0) \langle Q_{2u} v_e \rangle \qquad (7.27)$$

where Q_{2u} is the cross section for $(6^3P_2 \rightarrow 7^3S_1)$ transition and v_e is electron random velocity.

Equation (7.27) has been verified experimentally in Fig. 7.7. Where we have plotted intensities of the lines with i^2. The n_2 atoms are mainly produced by electron impact of ground level atoms, as this is the leading term in rate of production of n_2 atoms calculated in section 7.3.2, the intensity of lines will be proportional to n_e^2 ie to i^2. The plots I_{ul} vs. i^2 are straight lines as evident from fig. 7.7, where a plot of I_{ul} vs. i does not yield a straight line.

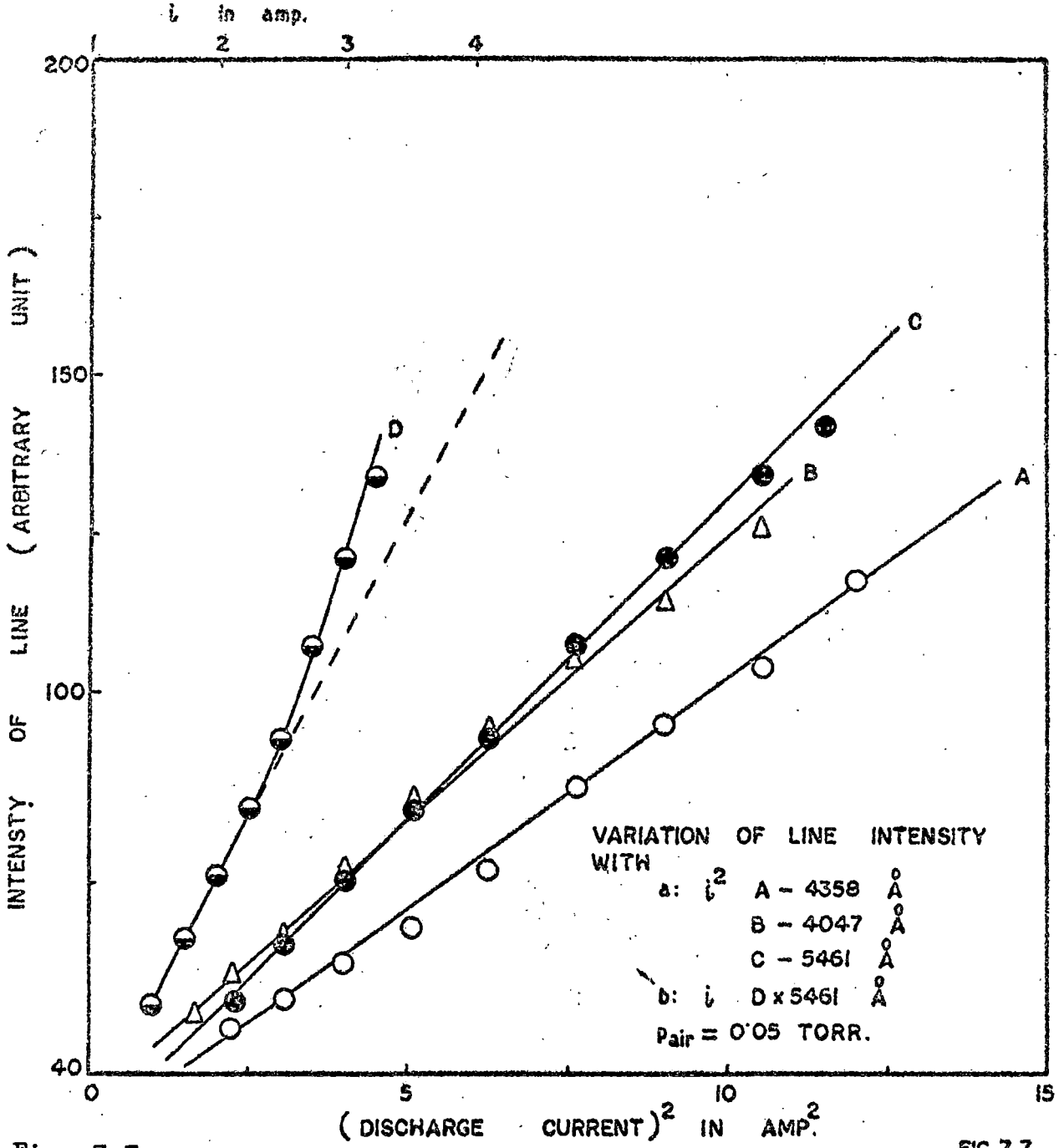

FIG.7.7.

Fig. 7.7.
Variation of spectral intensities of mercury arc with i^2 and i.

Hence equation (7.27) may be considered to be valid in the discharges concerned, if the value of n_u thus determined is put into eqn. (7.25) we get

$$\frac{\sum_3 (I_{ul})_B}{\sum_3 I_{ul}} = \frac{n_2(0)_B}{n_2(0)} \frac{n_e(0)_B}{n_e(0)} \frac{\langle Q_{2u} v_e \rangle_B}{\langle Q_{2u} v_e \rangle} \qquad (7.28)$$

Johnson and Hinnov (1969) have given a semi-empirical cross section for optically allowed transitions in helium,

$$Q_{ij}(i \to j) = 4 \left(\frac{E_H}{E_{ij}} \right)^2 f_{ij} \pi a_0^2 \left(\frac{E}{E_{ij}} \right)^{-1} \left[1 - \exp\left\{ -\beta \left(f_{ij} \frac{E_H}{E_{ij}} \right)^{-\gamma} \left(\frac{E}{E_{ij}} + 1 \right) \right\} \right] \ln \left(\frac{E}{E_{ij}} + \delta \right) \qquad (7.29)$$

where E is energy, E_{ij} is the threshold energy for transition and, β, γ and δ are non-negative, dimensionless, adjustable parameters. Griziniski's classical cross sections for $n \to n+1$ transition in hydrogen are adequately represented by the choice

$\beta = 1$, $\gamma = 0.4$ and $\delta = 0$. A choice $\beta = 1.2$, $\gamma = 0.7$, and $\delta = 0$, reproduces satisfactorily, M.J.Seaton's impact parameter cross section.

Considering a Maxwellian velocity distribution for electrons and utilising the cross section in eqn. (7.29)

we obtain

$$\langle Q_{ij}\, v_e \rangle = \left(\frac{8kT_e}{m\pi}\right)^{1/2} 4 \left(\frac{E_H}{E_{ij}}\right)^2 \pi a_0^2 f_{ij} \left(\frac{E_{ij}}{kT_e}\right)^2$$

$$\left[-\frac{1}{\frac{E_{ij}}{kT_e}} Ei\left(-\frac{E_{ij}}{kT_e}\right) + \frac{\exp\left[-\beta\left(f_{ij}\frac{E_H}{E_{ij}}\right)^{-\gamma}\right]}{\frac{E_{ij}}{kT_e} + \beta\left(f_{ij}\frac{E_H}{E_{ij}}\right)^{-\gamma}} \times \right.$$

$$\left. \times Ei\left(-\left[\frac{E_{ij}}{kT_e} + \beta\left(f_{ij}\frac{E_H}{E_{ij}}\right)^{-\gamma}\right]\right) \right]$$

Since $E_{ij} = 2.269$ eV. and $kT_e = 0.4$ eV,

$$\frac{E_{ij}}{kT_e} >> \beta\left(f_{ij}\frac{E_H}{E_{ij}}\right)^{-\gamma}$$

and asymptotic value of exponential integrals is given by Griem (1964) as

$$Ei(-x) \underset{x>5}{\longrightarrow} \frac{e^{-x}}{x}$$

the above expression becomes

$$\langle Q_{ij}\, v_e \rangle = \left(\frac{8kT_e}{m\pi}\right)^{1/2} 4 \left(\frac{E_H}{E_{ij}}\right)^2 \pi a_0^2 f_{ij}$$

$$\exp\left(-\frac{E_{ij}}{kT_e}\right)\left[1 - \exp\beta\left(f_{ij}\frac{E_H}{E_{ij}}\right)^{-\gamma}\right] \qquad (7.30)$$

Thus

$$\frac{\langle Q_{2u}\, v_e \rangle_B}{\langle Q_{2u}\, v_e \rangle} = \sqrt{\frac{kT_{eB}}{kT_e}} \exp E_{2u} \left(\frac{1}{kT_e} - \frac{1}{kT_{eB}} \right) \qquad (7.31)$$

From equation (7.28), (7.31) and (7.23), we get,

$$\frac{n_2(0)_B}{n_2(0)} = \frac{\sum (I_{ul})_B}{\sum I_{ul}} \left(\frac{kT_{eB}}{kT_e} \right)^{5/2} \exp E_{2u} \left(\frac{1}{kT_{eB}} - \frac{1}{kT_e} \right) \qquad (7.32)$$

From equation (7.32), we can determine the values of

$$n_2(0)_B \,/\, n_2(0)$$

and the values have been shown in Table 7.3. It is observed that as B increases, due to the coupled variation of $n_e(0)$ and T_e the value of $n_2(0)$ also increases at least upto a magnetic field of 1000 gauss.

TABLE 7.3.

Magnetic field B (Gauss)	T_e (eV)	$\frac{\sum (I_{ul})_B}{\sum I_{ul}}$	$\frac{n_2(0)_B}{n_2(0)}$
0	0.412	1.0	1.0
255	0.313	1.068	3.0
550	0.282	1.170	5.7
836	0.256	1.249	10.7
1050	0.243	1.293	15.6

7.4. Conclusions

The triplet radiation lines of mercury namely ($7^3S_1 \rightarrow 6^3P_{0,1,2}$) (λ 5461 Å, λ 4358 Å and λ 4047 Å) have the same upper level and consequently the intensity pattern of these lines should behave in a similar manner when a magnetic field is applied, but as it has been observed that the effect of magnetic field is different as regards the variation of intensity and the occurance of maxima in case of three lines it has been assumed after Le's et al (1961) that these variations can be explained by considering the reabsorption of the spectral lines. Considering this effect, an expression for $(I_{ul})_B / I_{ul}$ has been deduced. The slope of the line when $(I_{ul})_B / I_{ul}$ is plotted against $f_{lu}\lambda_{ul} \exp[-(E_n - E_o)/kT_{eB}]$ gives a value which is in close agreement with the theoretical calculated slope

$$\frac{1}{3}\pi r_o c R \left(\frac{M}{2\pi k T_g}\right)^{1/2} n_o(0)_B \, n_u(0)_B / n_u(0)$$

for two different discharge currents, justify the assumption that self absorption factor plays a dominent role in the intensity profile of these lines.

In the next section a detailed mathematical formulation has been presented showing a coupled variation of $n_e(0)$ with electron temperature. Utilising this relation an expression for the excited atom density

has been obtained interms of the total integrated intensity of the three lines and the electron temperature with and without magnetic field. The results indicate that due to coupled variation of electron density with electron temperature, the excited atom density increases with the magnetic field at least upto a field of 1000gauss. Increase of electron density has been observed in case of a glow discharge in a longitudinal magnetic field. The rate of increase is however, much higher than in case of glow discharge which shows that an arc plasma is much more affected by an external magnetic field.

References

1. Benson, R.S. and Kulander, J. L. (1972), Solar Physics, 27, 305.
2. Corney, A. (1977) Atomic and Laser Spectroscopy, Oxford University Press.
3. Cowan, R.D. and Diecke, G.H. (1948), Rev. Mod. Phys. 20 418.
4. Cummings, C.S. and Tonks, L. (1941) Phys. Rev. 59 514.
5. Forrest, J.R. and Franklin, R.N. (1966), Brit. J. Appl. Phys. 17 1569.
6. Forrest, J.R. and Franklin, R.N. (1969) J. Phys. B. Ser. 2, 2, 471.
7. Franklin, R. N. (1976) Plasma Phenomena in gas discharges (Oxford University Press).
8. Fujimoto, T. (1970) J. Phys. Soc. Japan 47 273, 265.
9. Griem, H.R. (1964), Plasma Spectroscopy (McGraw Hill, New York).
10. Gruzdev, P.F. (1967) Opt. Spectrosc. 22, 89.
11. Hearn, A.G. (1963) Proc. Phys. Soc. 81 648.
12. Hegde, M. S. and Ghosh, P.K. (1979) Physica 97C, 275.
13. Johnson, P.C., Cooke, M.J. and Allen, J.E. (1978) J. Phys. D. 11 1877.
14. Johnson, L.C. and Hinnov, E. (1969) Phys. Rev. 187 143.
15. Kulkarni, S.B. (1944) Curr.Sci. 13 254.
16. Les', Z. and Niewodniczan'ski, H. (1961) Acta. Phys. Polon 20 701.

17. Massey, H.S.W. (1971) Electronic and Ionic impact phenomena, Vol. 3 (Oxford University Press).

18. Mosberg (Jr.), E.R. & Wilkie, M.D. (1978) J.Q.S.R.T. 19 69.

19. Nakamura, Y. and Lucas, J. (1978) J. Phys. D. 11 325.

20. Nishikawa, M., Fujii-e, Y. and Suita, T. (1971) J. Phys. Soc. Japan 31 910.

21. Numano, M., Cussenot, J.R., Fabry, M. and Felden, M. (1975), J.Q.S.R.T. 15 1007.

22. Phelp, A.V. (1958) Phys. Rev. 110 1362.

23. Phelp, A.V. and McCoubrey, A.O. (1960) Phys. Rev. 118 1561.

24. Richter, J. (1968) in Plasma diognostics (Ed. Lochte-Holtgreven, W., North Holland Publishing Co., Amsterdam).

25. Rokhlin, G.N. (1939) Fiz. Zh. 1 347.

26. Sampson, D.H. (1969) Astrophys. J. 155 575.

27. Sen, S.N., Das, R.P. and Gupta, R.N. (1972) J. Phys. D. 5 1260.

28. Uvarov, F.A. and Fabrikant, V.A. (1965) Opt. Spectros. 18 323.

29. von-Engel, A. (1965) Ionised gases 2nd. Edn. (Oxford University Press).

30. Vriens, L., Keijser, R.A.J. and Ligthrt, F.A.S. (1978), J. Appl. Phys. 49 3807.